



HAL
open science

Gold nanoparticle-based supramolecular approach for dye-sensitized H₂-evolving photocathodes

Noémie Lalaoui, Mohamed Abdellah, Kelly L Materna, Bo Xu, Haining Tian, Anders Thapper, Jacinto Sa, Leif Hammarström, Sascha Ott

► **To cite this version:**

Noémie Lalaoui, Mohamed Abdellah, Kelly L Materna, Bo Xu, Haining Tian, et al.. Gold nanoparticle-based supramolecular approach for dye-sensitized H₂-evolving photocathodes. Dalton Transactions, 2022, 10.1039/D2DT02798D . hal-03812035

HAL Id: hal-03812035

<https://hal.science/hal-03812035v1>

Submitted on 12 Oct 2022

HAL is a multi-disciplinary open access archive for the deposit and dissemination of scientific research documents, whether they are published or not. The documents may come from teaching and research institutions in France or abroad, or from public or private research centers.

L'archive ouverte pluridisciplinaire **HAL**, est destinée au dépôt et à la diffusion de documents scientifiques de niveau recherche, publiés ou non, émanant des établissements d'enseignement et de recherche français ou étrangers, des laboratoires publics ou privés.

Gold Nanoparticle-based Supramolecular Approach for Dye-sensitized H₂-Evolving Photocathodes

Received 00th January 20xx,
Accepted 00th January 20xx

Noémie Lalaoui,^{#,a,b} Mohamed Abdellah,^{#,a,c} Kelly L. Materna,^a Bo Xu,^a Haining Tian,^a Anders Thapper,^a Jacinto Sa,^{a,d} Leif Hammarström,^{*,a} and Sascha Ott^{*,a}

DOI: 10.1039/x0xx00000x

Solar conversion of water into the storable energy carrier H₂ can be achieved through photoelectrochemical water splitting using light adsorbing anodes and cathodes bearing O₂ and H₂ evolving catalysts, respectively. Herein a novel photocathode nano hybrid system is reported. This photocathode consists of a dye-sensitized p-type nickel oxide (NiO) with a perylene-based chromophore (PCA) and a tetra-adamantane modified cobaloxime reduction catalyst (Co) that photo-reduces aqueous protons to H₂. An original supramolecular approach was employed, using β-cyclodextrin functionalized gold nanoparticles (β-CD-AuNPs) to link the alkane chain of the PCA dye to the adamantane moieties of the cobaloxime catalyst (Co). This new architecture was investigated by photoelectrochemical measurements and via femtosecond-transient absorption spectroscopy. The results show that irradiation of the complete NiO|PCA|β-CD-AuNPs|Co electrode leads to ultrafast hole injection into NiO (τ = 3 ps) from the excited dye, followed by rapid reduction of the catalyst, and finally H₂ evolution.

Introduction

The development of sustainable energy technologies that allows us to decrease our use of fossil fuels, with their negative environmental impact, is one of the greatest challenges of our times. Inspired by natural photosynthesis, the conversion of solar energy into fuels (e.g. H₂, CH₄, CO) from abundant substrates (H₂O, CO₂) by photoelectrochemical cells (PECs) is a promising strategy to address this challenge.¹⁻⁴ The electrodes in dye-sensitized photoelectrochemical cells (DS-PECs) are typically based on a wide band gap semiconductor that is sensitized with molecular dye molecules as light harvesting compounds⁵⁻⁸ and catalysts for solar fuel production.^{9, 10} In a complete tandem cell, water oxidation occurs at the photoanode, while H₂ is produced at the photocathode.

Significant work has been done to improve the photoanodes, which can now achieve relatively high photocurrents and efficiencies.^{5, 7, 8} In comparison, the photocathodes have been less explored, and their performances are currently limiting the efficiency of complete DS-PECs.^{6, 11-13} In dye-sensitized photocathodes (DS-PCs), light absorption by the surface bound dye is followed by hole injection into the valence band of the semiconductor, creating a reduced dye that can transfer an electron to the co-immobilized catalyst. Two reducing equivalents as well as two protons are needed by the catalyst to form H₂. Rapid charge recombination relative to the rate of proton reduction limits the overall efficiency of DS-PCs. To generate higher photocurrents, the dominant recombination mechanisms between holes in the p-type semiconductor and (1) the reduced dye or (2) the reduced catalyst must be prevented.¹²

^a Department of Chemistry-Ångström Laboratories, Uppsala University, Box 523, SE75120 Uppsala, Sweden. E-mail: leif.hammarstrom@kemi.uu.se; sascha.ott@kemi.uu.se

^b UMR CNRS 6521, Université de Bretagne Occidentale, 6 avenue Le Gorgeu, CS93837, 29238 Brest, Cedex3, France.

^c Department of Chemistry, Qena Faculty of Science, South Valley University, 83523 Qena, Egypt.

^d Institute of Physical Chemistry, Polish Academy of Sciences, 01-224 Warsaw, Poland.

[#] These authors contributed equally to this work

† Electronic Supplementary Information (ESI) available. See DOI: 10.1039/x0xx00000x

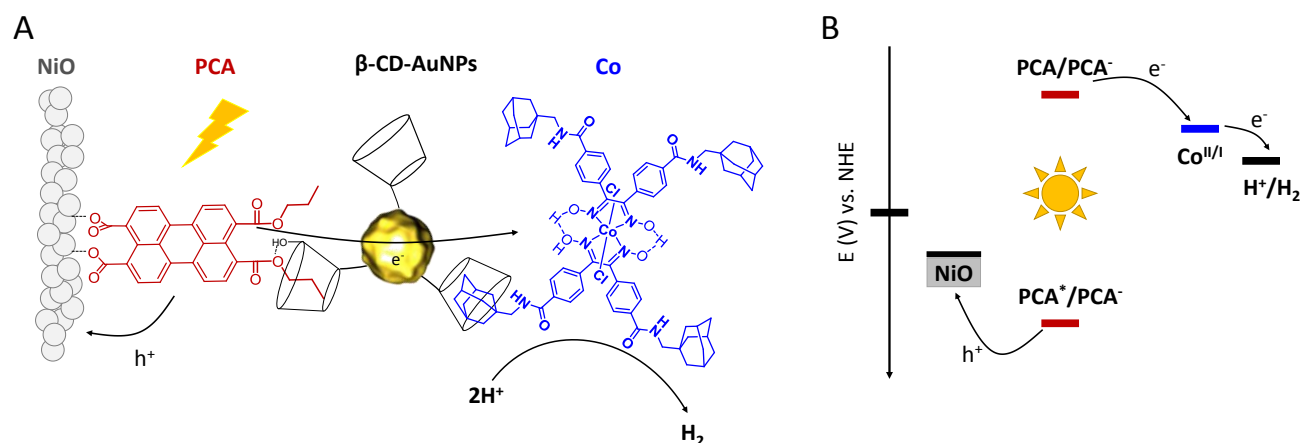


Figure 1. A) Representation of the PCA| β -CD-AuNPs|Co supramolecular assembly anchored onto a mesoporous NiO thin film, B) Energy diagram of the photocathode.

Semiconductor, electrolyte, and the dye, by which photoexcitation and catalyst are arranged on the electrode surface greatly impact the performance of DS-PCs. Several DS-PCs photocathodes have been described with the majority relying on NiO substrates.^{6, 14-26} However, problems associated with the high density of traps and low hole mobility have been identified,²⁷⁻³⁰ and other p-type metal oxide semiconductors such as LaFeO₃ and CuCrO₂ have been recently proposed as alternative materials for the construction of DS-PC for solar-driven H₂ generation.³¹⁻³³ As far as the dye is concerned, organic chromophores and ruthenium based complexes are the two families of light-harvesting units that are frequently used. The best photosensitizers have a donor–bridge–acceptor structure, where the HOMO is positioned close to the anchoring group and the LUMO is positioned away from the NiO surface.^{13, 34-36} This push–pull structure is thought to promote charge-separation and slow down charge recombination by keeping the electron on the reduced dye physically distant to the holes in the NiO. Among organic chromophores, perylene-based dyes are renowned for their high stability and intense visible light absorption. PMI based photocathodes have been assembled with heterogeneous catalysts,³⁵ molecular catalysts in solution³⁷ and immobilized Ni(P₂N₂)₂ – based catalysts,^{26, 33} but to our knowledge, never with a cobaloxime type catalysts.

To improve PC performance, many PC designs have focused on optimizing the electrode assembly. The different strategies are DS-PCs combined with a catalyst in solution,^{16, 34, 37} co-grafted dye/catalyst systems,^{6, 19, 22, 38} layer by layer assemblies of the dye and the catalyst,^{17, 18, 20} and supramolecular or covalent dye/catalyst assemblies.^{14, 15, 21, 23}

In this study, we report the design and synthesis of a new dye/catalyst supramolecular assembly based on β -cyclodextrin functionalized gold nanoparticles (β -CD-AuNPs) that connect a perylene-based dye (PCA) to a cobaloxime catalyst (Co). A rational and simple procedure of sequential immersion of NiO films into solutions of PCA, β -CD-AuNPs and Co was employed to produce electrodes of the type NiO|PCA| β -CD-AuNPs|Co (Figure 1A) where the catalyst is spatially separated from the

recombination of electron energy, to the adamantane moiety of the dye and the adamantane moiety of the catalyst to form the supramolecular assembly. Cyclodextrin has been previously used to form host-guest interactions in order to immobilized molecular catalysts on electrode surfaces.^{39, 40} In the present architecture, AuNPs are proposed to act as electron transfer bridges by accepting electrons from PCA and transporting them to Co. This function of the AuNPs is motivated by previous studies in which such constructs were shown to enhance electron transfer rates at protein/electrode interfaces in bioelectrochemical systems.^{41, 42} Other studies have shown that small gold nanoparticles (2-3 nm) significantly increase charge separation in chromophore-gold nano-assemblies, where the charge separation is sustained for several microseconds before undergoing recombination.^{43, 44} However, to the best of our knowledge, this strategy has never been explored to develop operative photocathodes for H₂ evolution.

Results and discussion

Synthesis and characterization

PCA,⁴⁵ β -CD-AuNPs^{46, 47} and [Co(dcpGH)(dcpGH₂)]Cl₂⁴⁸ **1** were synthesized as previously reported. The adamantane moiety was added to **1** via peptide coupling (see SI) to afford Co. The target complex was characterized by ¹H NMR, Fourier transform infrared (FT-IR) spectroscopy, high-resolution mass spectrometry (HR-MS) and electrochemistry (Figure S1- S3). Figure S11 shows a transmission electron microscopy (TEM) image of the functionalized AuNPs and reveals an average AuNP size of 3.2 ± 0.7 nm, which is in good agreement with previous studies.⁴⁷ This type of AuNPs was selected to form a supramolecular assembly due to the cyclodextrin moieties which are able to interact with a variety of guests.⁴⁹ The PCA dye was selected for its ability to interact with both NiO and β -CD. The monoanhydride precursor of PCA opens to form the dicarboxylate when exposed to metal oxide semiconductors

for convenient electrode functionalization,⁵⁰ while the hydrophobic alkane chain can interact with the β -CD moiety of the AuNPs, as illustrated in Figure 1A. For short alkane chain, a host : guest ratio of 1:1 is expected.⁵¹ The optical and electrochemical properties of PCA are display in Table 1. The dye anion exhibits sufficient driving force ($E_{PCA/PCA^-} = -0.91$ V vs. NHE) to reduce **Co** to a catalytically active state ($E_{Co,onset} = -0.38$ V vs. NHE).⁵² Hole injection into the valence band of NiO ($E \approx 0.46$ V vs. NHE) is facilitated by the highly anodic excited state reduction potentials ($E_{PCA^*/PCA^-} = +1.73$ V vs. NHE). PCA

displays a broad absorption from 450 to 550 nm with a maximum at 503 nm and a shoulder at 476 nm (Figure S6). The intense visible light absorption and favourable electrochemical properties of PCA are well suited for the application of the dye in DS-PCs with **Co** as the catalyst (Figure 1B). To confirm this ability to reduce the immobilized catalyst, PCs were assembled for photoelectrochemical analysis.

Table 1. Optical and electrochemical properties

	λ_{max}^a	ϵ^a ($M^{-1} cm^{-1}$)	E_{red} (V vs. Fc^+/Fc)	E_{ox} (V vs. Fc^+/Fc)	E_{red} (V vs. NHE) ^e	E_{ox} (V vs. NHE) ^e
PCA ^{c,d}	503 476	36000 29300	-1.64	1	-0.91	1.73
Co ^b	-	-	-1.13	-0.4	-0.4	0.33

^a Adsorption spectra in CH_2Cl_2 . Redox potentials obtained in a DMF^b or in a CH_3CN ^c solution. ^d Redox potentials obtained for surface bound molecules. ^e Redox potentials referred to NHE by addition of 730 mV.⁵³

Electrode preparation and pre-catalysis characterization.

PCA, β -CD-AuNPs, and **Co** were used to prepare a photocathode for H_2 evolution based on FTO coated NiO films.^{26, 54} NiO electrodes were prepared by immersion into a solution of PCA (0.2 mM) in a mixture of CH_2Cl_2 and methanol (1:1) for 24 hours to give NiO|PCA.

Co was immobilized on the NiO|PCA photocathodes in a layered assembly using β -CD-AuNPs to link the alkane chain of the dye to the adamantane moiety of the catalyst. Sequential loading of molecules was carried out by soaking the NiO|PCA films in an aqueous solution of β -CD-AuNPs (0.5 mg mL⁻¹) for 1h to give NiO|PCA| β -CD-AuNPs, followed by soaking in a **Co** solution (0.2 mM in MeOH-1%DMF) for 30 minutes to afford NiO|PCA| β -CD-AuNPs|**Co** electrodes

Control electrodes without β -CD-AuNPs (denoted as NiO|PCA+**Co**) were obtained by soaking the NiO|PCA films in a **Co** solution following the same protocol. All immobilization steps were carried out at room temperature in the dark (see experimental part for details). The absorption spectra of the sensitized electrodes are depicted in Figure 2B. UV-vis spectra of the films show the characteristic visible light absorption

profiles of the dye. NiO|PCA electrodes display a blue shift and higher intensity for the peak at 448 nm than at 503 nm as opposed to the solution-based experiments (Figure S6 and S9). This is attributed to the anhydride opening and the binding of the carboxylates to NiO.^{55, 56} β -CD-AuNPs binding was confirmed by UV-vis spectroscopy. In aqueous solution (Figure 2A) a relatively weak plasmon resonance absorption maxima at 507 nm is observed.⁴⁷ The difference absorption spectrum of NiO|PCA and NiO|PCA| β -CD-AuNPs electrodes (Figure 2C) exhibits a peak at 538 nm attributed to the surface plasmon resonance of immobilized β -CD-AuNPs.

The immobilization of the β -CD-AuNPs and the catalyst does not affect the NiO|PCA interface. The amount of dye loading on the photoelectrode was quantified by measuring the UV-Vis spectra of PCA solution after sensitization of NiO films. A surface coverage of 20 ± 2 nmol cm⁻² was found, which is in the same range as those determined in previous studies using similar electrodes.⁵⁷ The amount of catalyst loading on the photoelectrodes was quantified by ICP-OES after acid digestion of the electrodes. A coverage of 0.5 ± 0.3 nmol cm⁻² was found for NiO|PCA| β -CD-AuNPs|**Co** electrodes. No catalyst was observed for the NiO|PCA+**Co** electrodes

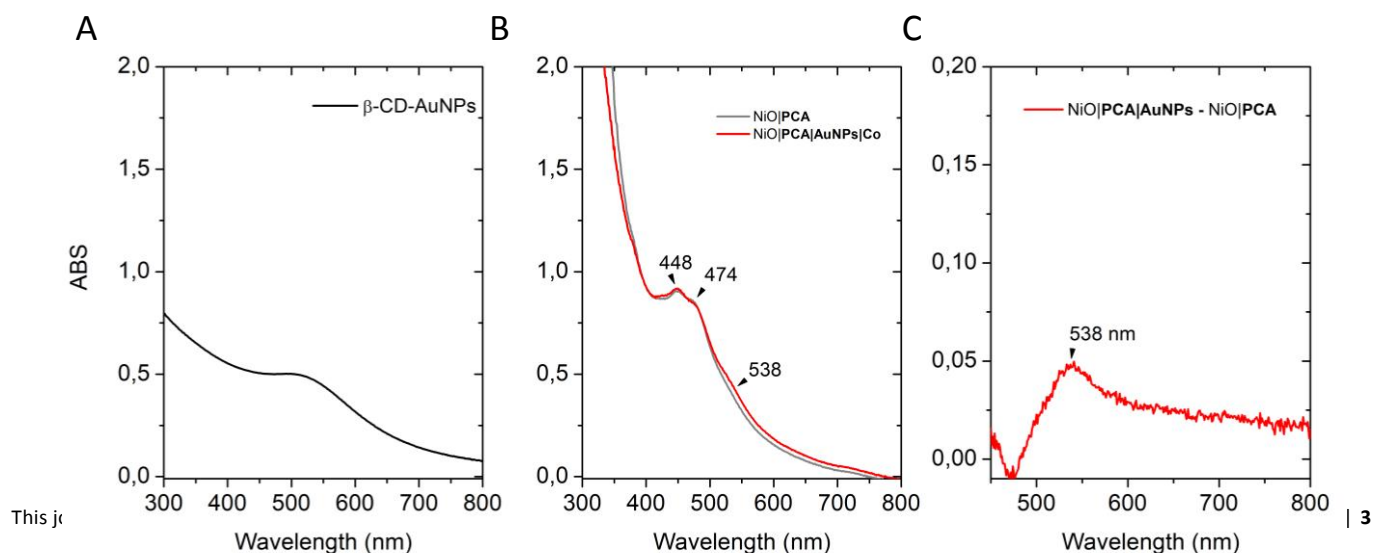


Figure 2. Absorption UV-Vis spectrum of A) an aqueous solution of β -CD-AuNPs, B) NiO|PCA (grey) and NiO|PCA| β -CD-AuNPs|**Co** (red) electrodes (NiO electrodes were used to set the background), and C) Difference

confirming the crucial role of β -CD-AuNPs for the immobilization of Co catalysts.

The presence of PCA, β -CD-AuNPs and Co at the surface of NiO electrodes was further investigated by XPS analyses. The survey spectrum of the NiO electrodes (Figure S12) shows peaks attributed to Ni 2p and NiLMM Auger photoelectrons. After chemisorption of PCA onto NiO, the survey spectrum of the resulting material NiO|PCA shows an increase in the level of C and O compared to the NiO electrodes, consistent with the presence of PCA (Figure S13). The survey spectrum of NiO|PCA| β -CD-AuNPs|Co electrodes (Figure S14) shows the same features, but also additional information such as the presence of N and Au. A signal in the 398–402 eV range of the N 1s core level region (Figure S13) corresponds to N atoms present in grafted Co. The doublets for Au 4f_{7/2} (83.8 eV) and Au 4f_{5/2} (87.5 eV) shown in Figure S14 are characteristic of Au⁰ of the β -CD-AuNPs.^{58, 59} The absence of a signal at 84.9 eV as found for Au^I in a gold octanethiol complex⁶⁰ indicates that the gold atoms in the clusters are largely present as Au⁰. Further substantiation can be found on Au 4f peaks with slight asymmetry consistent with the presence of small nanoparticles/cluster.⁶¹ Au⁰ peaks due to metallic conduction (i.e. non-occupied states at the Fermi level) should be asymmetric with a tailing towards higher binding energy. XPS data clearly evidence the immobilization of PCA, β -CD-AuNPs and Co at the surface of NiO electrodes.

Photoelectrochemistry with NiO|PCA and NiO|PCA| β -CD-AuNPs

To ensure that NiO|PCA| β -CD-AuNPs electrodes could function without the kinetic limitations of sluggish catalyst reactions and charge recombination, photoelectrochemical measurements were performed in the presence of a soluble irreversible electron acceptor (IEA) in solution (Figure 3A). Linear sweep voltammetry (LSV) was carried out in MES buffer electrolyte (0.1M, pH 5), at room temperature in an Ar-purged one compartment three electrodes electrochemical cell using a Pt counter electrode and a Ag/AgCl reference electrode. Irradiation of NiO|PCA and NiO|PCA| β -CD-AuNPs electrodes resulted in only minor photocurrents without a soluble acceptor (Figure 3A). Addition of the IEA chloropentamminecobalt(III) chloride (10 mM) in the electrolyte solution allows for estimation of a maximal attainable photocurrent as [Co^{III}(NH₃)₅Cl₂]Cl is known to be irreversibly reduced in solution.⁶² The IEA allows the photo-reduced dye to dispose its photoelectrons and to regenerate the ground state, thereby limiting the effects of reductive dye decomposition and charge recombination, thereby enhancing the photocurrent response for NiO|PCA and NiO|PCA| β -CD-AuNPs electrodes dramatically (Figure 3A).

With NiO|PCA| β -CD-AuNPs electrodes, an absolute photocurrent response of $|I| \approx 420 \mu\text{A cm}^{-2}$ (0.0 V vs. Ag/AgCl) was observed, which indicates efficient light induced hole

injection from the dye to the valence band of NiO with reduction of the IEA by PCA⁻. For comparison, NiO|PCA electrodes displayed a lower maximum photocurrent ($|I| \approx$

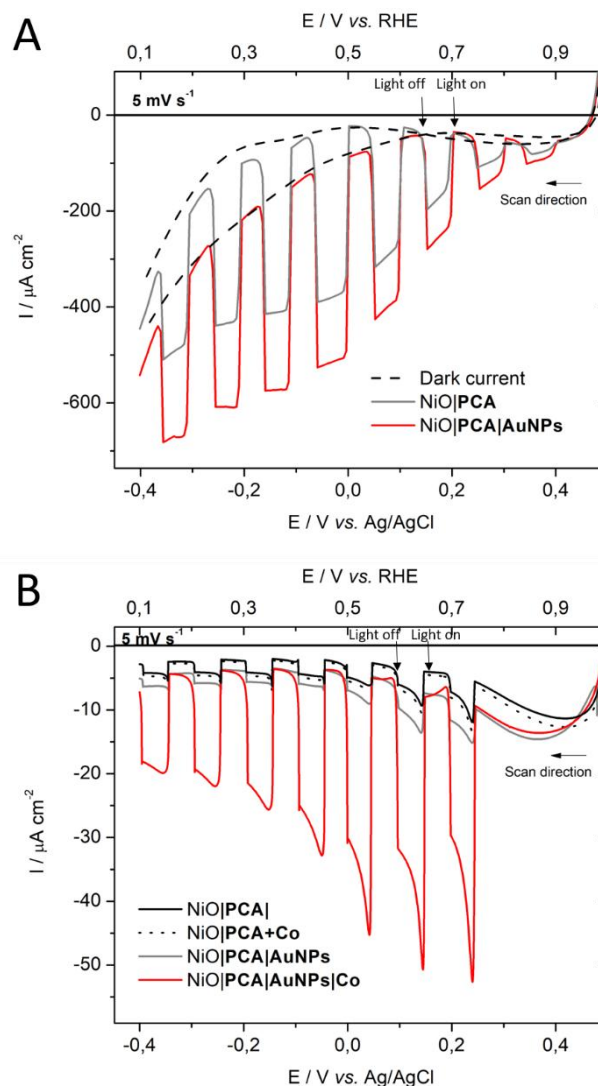


Figure 3. Linear sweep voltammograms (LSVs) under chopped light illumination of A) NiO|PCA (grey) electrodes, and NiO|PCA| β -CD-AuNPs (red) electrodes with 10 mM of Co^{III}(NH₃)₅Cl₂]Cl acceptor in solution. B) LSV scans of NiO|PCA, NiO|PCA| β -CD-AuNPs, NiO|PCA+Co and NiO|PCA| β -CD-AuNPs|Co. All experiments were performed in MES buffer (0.1M, pH5). Illumination with a white LED with 100 mW of 1 cm^{-2} . An active electrode area of 1 cm^{-2} was used with a scan rate of 5 mV s^{-1} .

are present. This finding supports that co-anchoring a catalyst could be a viable approach to exploit the reductive power of NiO|PCA| β -CD-AuNPs electrodes for H₂ photo-production.

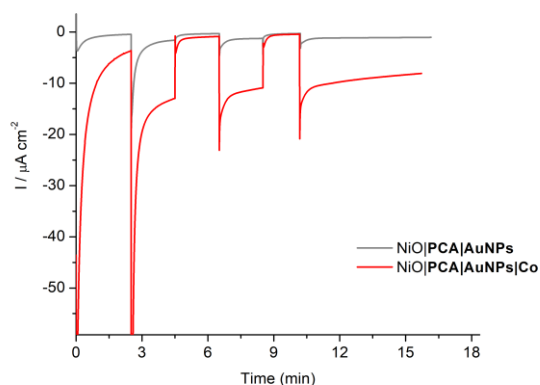


Figure 4. Chopped-light chronoamperometric measurements of NiO|PCA| β -CD-AuNPs and NiO|PCA| β -CD-AuNPs|Co photocathodes at an applied bias of -0.1 V vs. Ag/AgCl in pH 5 MES buffer.

The photoelectrochemical properties of the NiO|PCA| β -CD-AuNPs|Co photocathodes were evaluated in aqueous solution (0.1 M MES buffer, pH 5). Linear sweep voltammograms were recorded under chopped light irradiation (Figure 3B). Immobilization of Co catalyst on the electrode resulted in a 10-fold photocurrent increase compared to that of NiO|PCA| β -CD-AuNPs electrodes ($|j| = 15.8 \mu\text{A cm}^{-2}$, -0.2 V vs. Ag/AgCl). This enhanced response is attributed to the ability of PCA⁻ to reduce Co and ultimately protons. The absence of current enhancement in the control experiment confirmed the crucial role of β -CD-AuNPs for the immobilization of Co catalysts.

Chronoamperometric measurements were performed under chopped light irradiation at -0.1 V vs. Ag/AgCl over a period of 15 min showing steady-state cathodic photocurrent (Figure 4) with a current density of ca. $-11 \mu\text{A cm}^{-2}$. Photoelectrochemical H₂ generation was confirmed by long term electrolysis over a period of 1 h (Figure S16), during which the magnitude of the current decreases slowly.

Clark electrode measurements confirmed the evolution of hydrogen in solution during the chronoamperometric measurements with a faradic efficiency of 10 ± 2 % and a TON of 8. Noteworthy is that these measurements do not take into account H₂ present in the headspace.⁶³ Moreover, no H₂ generation was observed in the absence of catalyst or in the absence of light. This relatively low yield is within the current state-of-the-art in NiO-based dye-sensitized H₂-evolving photocathodes,³² and can be attributed in part to the low catalyst loading (Table S1). We attempted to increase the catalyst loading by increasing the immersion time of the electrodes in the catalyst solution. Longer immersion times led

to PCs exhibiting smaller photocurrents (data not shown). The decrease in the photocurrent (from 9.8 to $4 \mu\text{A cm}^{-2}$) observed during long-term electrolysis can be attributed partly to some leaching or demetalation⁶⁴ of the catalyst since we observed a decrease of catalyst loading by ICP measurements after photoelectrochemical measurements (Table S1). Dye

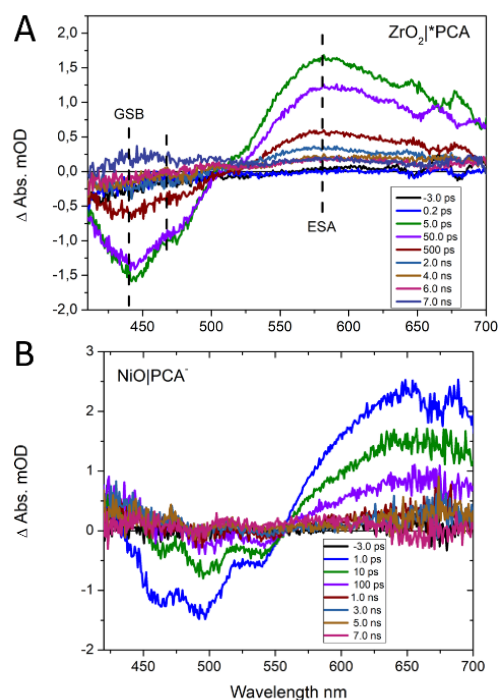


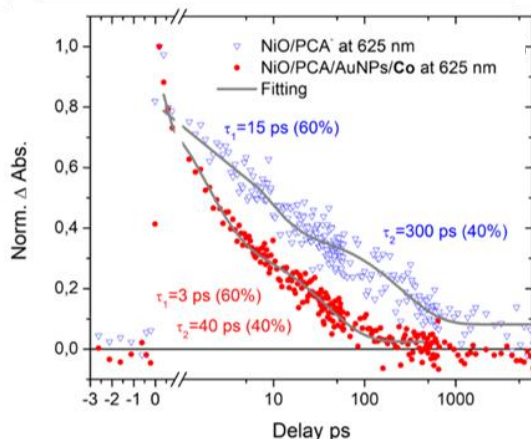
Figure 5. fs TA spectra of A) ZrO₂|PCA and B) NiO|PCA, after excitation at 440 nm.

aggregation and competing reactions, such as NiO reduction^{15, 65, 66} may also be considered.

Transient absorption spectroscopy

Femtosecond transient UV/Vis absorption measurements were conducted on NiO|PCA, NiO|PCA| β -CD-AuNPs, and NiO|PCA| β -CD-AuNPs|Co photocathodes to understand the charge dynamics upon PCA excitation. Energetically, hole injection is possible from excited PCA dye to the NiO valence band.⁶⁷ The excited state dynamics of PCA in NiO|PCA was compared to that of a ZrO₂|PCA reference system, in which neither electrons nor holes can be injected due to the high-energy conduction band and low-energy valence band of ZrO₂.⁶⁸ Figure 5 shows the transient absorption spectra of the PCA dye attached to ZrO₂ and NiO at different time delays after excitation. Both sets of spectra display the ground state bleach of the PCA dye at around 420 to 550 nm. The spectra of the ZrO₂|PCA system shows an excited state absorption (ESA) from 550 to 750 nm with a distinct maximum around 580 nm, as expected.⁵⁰ In NiO|PCA, the induced absorption is seen further to the red, without a distinct maximum. This difference agrees with the difference spectrum after

spectroelectrochemical reduction of the NiO-bound dye (Figure S10). Figure S18 presents the kinetic traces associated with ESA (probed at 580 nm) in $\text{ZrO}_2|\text{PCA}$, and the reduced dye in $\text{NiO}|\text{PCA}$ (probed at 625 nm), both of which were fitted with a double-exponential function.



Clearly, attaching PCA to NiO ($\tau_1 = 15$ ps (60%), $\tau_2 = 300$ ps (40%)) results in faster dynamics than having the dye on ZrO_2 ($\tau_1 = 30$ ps (60%), $\tau_2 = 500$ ps (40%)).³⁷ This is attributed to the photo driven hole injection from excited PCA into the NiO valence band.³⁷ The thereby produced charge separated state $\text{NiO}^+|\text{PCA}^-$ is however very short lived, and recombines to the ground state on the picosecond timescale, giving rise to the observed overall faster kinetics in $\text{NiO}|\text{PCA}$ compared to that

Figure 6. Time traces of $\text{NiO}|\text{PCA}^-$ (blue triangles) and $\text{NiO}|\text{PCA}|\text{AuNPs}|\text{Co}$ (red dots) at 625 nm (reduced dye).

in $\text{ZrO}_2|\text{PCA}$. The photoelectrochemical properties the $\text{NiO}|\text{PCA}|\beta\text{-CD-AuNPs}|\text{Co}$ photocathodes (Figure 3B) shows the role of the Au NPs as an important structural component in the supramolecular system. Figure S17C presents the TA spectra of the $\text{NiO}|\text{PCA}|\beta\text{-CD-AuNPs}|\text{Co}$ photocathode which qualitatively contains the same features as those of $\text{NiO}|\text{PCA}$, but clearly with even shorter lifetimes of the signal that is attributed to the reduced PCA. Figure 6 presents the kinetic traces of the decay of the reduced dye in $\text{NiO}|\text{PCA}|\beta\text{-CD-AuNPs}|\text{Co}$ photocathodes, with a fit ($\tau_1 = 3$ ps (60%), $\tau_2 = 40$ ps (40%)), in comparison with the same features in $\text{NiO}|\text{PCA}$. In addition to the fast dynamic that is caused by attaching the dye to NiO (due to the hole injection and recombination), directed electron transfer from the reduced PCA via $\beta\text{-CD-AuNPs}$ to the catalyst results in even faster dynamics of PCA^- (Figure 6). On one hand, inserting the $\beta\text{-CD-AuNPs}$ will improve the loading of the catalyst and at the same time, it will guide the electron transfer from the reduced dye to the catalyst. Spectroscopically, it was not possible to detect the reduced form of the Co catalyst due to its comparably weak spectroscopic features compare to the dye GSB.⁶⁹

Conclusions

Here, we report the first supramolecular assembly based on cyclodextrin functionalized gold nanoparticles for the construction of a NiO-based photocathode for H_2 evolution from water. $\beta\text{-CD-AuNPs}$ play a crucial role in the immobilization of Co catalysts and guide the electron transfer from the reduced dye to the catalyst. It was shown that light irradiation initiates an electron transfer from the NiO to the dye molecule, and subsequently from the reduced dye to the catalyst. The photocathode produces H_2 with a Faradic efficiency of 10%, which is in the same range as those of previously reported molecular photocathodes based on cobaloxime catalysts.³² Further work to improve this system will target the use of novel p-type transparent materials such as CuCrO_2 , which have already proved promising.^{32,33}

Experimental

Materials.

All chemicals were purchased from commercial suppliers (Sigma-Aldrich, VWR and Alfa-Aesar) and used without further purification, unless stated otherwise. Solvents were dried using drying agents and freshly distilled under argon before use. All organic reactions were performed under inert argon atmosphere.

Instrumentation.

^1H NMR spectra were measured on a JEOL Eclipse 400 MHz spectrometer. High-resolution mass spectral analyses (HRMS) were performed on a pneumatically-assisted electrospray ionization Fourier transform (FTMS+pNSI) mass spectrometer (orbitrapXL). UV-Vis spectroscopic measurements were collected using a Varian Cary 50 Bio UV-Vis spectrophotometer. Attenuated total reflectance Fourier transform infrared (ATR-FTIR) spectroscopic measurements were performed using a Perkin Elmer Spectrum One FTIR-Spectrometer with a Perkin Elmer Universal ATR Sampling Accessory. Inductively Coupled Plasma-Optical Emission Spectrometry (ICP-OES) experiments were performed using a Perkin Elmer Optical Emission Spectrometer. X-ray photoelectron spectroscopy (XPS) spectra were recorded on a PHI Quantera II scanning XPS microprobe with monochromated Al K α radiation (1486.6 eV). Survey spectra were captures at a pass energy of 224 eV, while for high-resolution spectra a pass energy of 55 eV was used. All spectra were referenced against an internal signature (C 1s, 284.8 eV). Transmission electron microscopy (TEM) images were obtained using JEOL JEM 1400 instrument. The particle size distribution was obtained from digitalized amplified micrographs by averaging the larger and smaller axis diameters measured in each particle.

Electrochemical and photoelectrochemical measurements were acquired with an Autolab potentiostat (PGSTAT 302N). Electrochemical measurements were conducted in a traditional three-electrodes system with Ag/AgNO_3 reference electrode, a platinum rod as counter electrode and either

glassy carbon or FTO/NiO as working electrodes. Ferrocene was used as an internal standard and all the potentials converted into the Normal Hydrogen Electrode using $E_{Fc+/Fc} = 0.64$ V vs.NHE. LED lamp (cool white, 5000K) was used as light source. A Unisense Clark electrode H_2 sensor was used for the detection and the quantification of H_2 . A Dektak150 Surface Profiler was used to measure the NiO film thicknesses.

TA spectroscopy

Femto-second transient absorption spectroscopy (fs-TAS) was performed probing in the UV-Vis region using a Newport TAS. A Coherent Libra Ti:sapphire amplifier (1.5 mJ, 3kHz, 800 nm, fwhm 40 fs) was used and split into pump and probe beams. An excitation wavelength of 440 nm was generated by directing the pump beam into the optical parametric amplifiers (TOPAS-Prime and NIRUVVIS, Light Conversion) and then focused and centered on the dry films with a pump power adjusted to 500 μ W. The 800 nm fundamental of the amplifier was focused on a CaF_2 crystal (Newport TAS), generating the white light supercontinuum probe. A silicon diode array (Newport custom made) was used to record the probe spectrum. A mechanical chopper blocked every other pump pulse, and the transient absorption at each time point was calculated for an average of 1000 ms chopped/un-chopped pulse pairs. To record the transient absorption spectra at different time points, an optical delay line was used to scan the delay of the probe beam relative to the pump beam from -5 ps to 7.5 ns. A total of 10-15 scans were collected and averaged for each sample. Prior to analysis, the data was corrected for the spectral chirp using Surface Xplorer 4.2, where single wavelength fits were also performed.

Synthesis

$[Co(dcpGH)(dcpGH_2)Cl_2]^{52}$ ($dcpGH_2$ = diphenylglyoxime-4,4'-dicarboxylic acid) **1**, PCA dye⁴⁵ and β -CD-AuNPs^{46, 47} were synthesized according to literature method.

Synthesis of **Co** (Benzotriazol-1-yloxy)tripyrrolidinophosphonium hexafluorophosphate (PyBOP, 4 equiv., 0.51 mmol) was added to a solution of **1** (1 equiv., 0.13 mmol), diisopropylethylamine (7 equiv., 0.90 mmol) and 1-Adamantanemethylamine (4 equiv., 0.51 mmol) dissolved in DMF (7 mL). Upon addition, 1-Adamantanemethylamine became completely soluble. The reaction mixture was then stirred at R.T. overnight. DMF was removed under reduce pressure and the resulting oil was dissolved in 10 mL of CH_2Cl_2 . The organic phase was washed with brine (2 x 5 mL), water (2 x 5 mL), dried ($MgSO_4$), filtered and reduced to 2 mL. Then the crude orange product was precipitated with Et_2O , filtered and washed with Et_2O . The solid was purified by flash chromatography (0 to 7 % methanol in CH_2Cl_2). The pure product was obtained after evaporation of the solvent in combine fractions to give **2** as an orange solid (83 mg, 46 %). 1H NMR (CD_2Cl_2 , 400 MHz): δ (ppm) 19.25 (Br, 2H, oxime), 7.51 – 7.26 (m, 16H, Ar), 7.10 (s, 4H, NH amide), 3.08 (s, 8H, CH_2), 1.94 (s, 12H, CH adamantane), 1.68-1.52 (m, 48H, CH_2 adamantane). HR-MS (ESI⁺): m/z, 1302.6 [M-H-2Cl]⁺.

Electrode Preparation

First, FTO-coated glass slides were cleaned via sequential sonication steps using detergent, acetone, and isopropanol. Then, NiO was screen printed onto the clean FTO coated glass using a NiO paste as previously reported.^{54, 70} After each layer of screen printing, the electrodes were annealed at 120 °C for 9 minutes on a hot plate. Three layers were screen printed and were finally annealed at 450 °C for 30 minutes in an oven, resulting in a thickness of ~ 1.2 μ m determined by profilometry.

Photocathode Assemblies.

NiO electrodes were soaked in a 1:1 CH_2Cl_2 :MeOH solution of PCA (0.2 mM) for 24h at room temperature, then rinsed with CH_2Cl_2 ; MeOH and dried in air affording NiO|PCA electrodes. For the molecular assemblies PCA| β -CD-AuNP|Co, sequential loading of molecules was carried out by soaking the films in aqueous solution of β -CD-AuNPs (0.5 mg mL⁻¹) for 1h (giving NiO|PCA| β -CD-AuNPs electrodes), followed by soaking in methanol-1%DMF solution of the catalyst Co (0.2 mM) for 0.5 h. The electrodes were then rinsed with MeOH-1%DMF solution and dried in air. Water and methanol were used to rinse the films between the two loading solutions. NiO|PCA|Co electrodes were obtained following the same procedure without the soaking step in solution of β -CD-AuNPs.

Surface loading quantification.

Surface coverage (Γ in mol/cm) of PCA was evaluated by measuring the UV-vis spectra of PCA solution before and after sensitization of NiO films. A surface coverage of 20 ± 2 nmol cm⁻² was found.

Co was quantified by ICP-OES after digestion of NiO photocathodes in a mixture of conc. H_2SO_4 (1 mL) and HNO_3 (1mL) by heating in a Biotage (Uppsala Sweden) SPX microwave reactor for 10 min at 100 °C. The resulting clear solution was filtered with a micron filter syringe, then diluted using deionized water and analyzed by ICP-OES (pre-calibrated with known concentrations of each element (sulfur and cobalt) of interest). The geometric surface areas of the dissolved electrodes were measured prior to being digested in order to determine the surface loading.

Photoelectrochemistry measurement.

All the PEC experiments were performed in 0.1 M MES buffer at pH 5 using an Ag/AgCl (sat'd NaCl) reference electrode and a Pt wire counter electrode. Linear sweep voltammetric measurements were performed in a one-chamber cell degassed with Ar. A white LED was used to illuminate the photocathode, to generate a power density of approximately 100 mW/cm². Long term chronoamperometric experiments were performed in an H-cell in order to avoid leakage from the Pt counter electrode onto the working electrode. The photocathode and the reference were in one compartment, while the Pt counter electrode was in the other one. All samples were degassed under Ar prior to measurements.

Clark electrode H₂ measurements.

H₂ detection using a Clark electrode was performed based on a previously reported method.⁶³ Prior to measurements, the Unisense Clark electrode was calibrated using known concentrations of dissolved H₂ in 0.1 M MES buffer at pH 5 and measuring the Clark electrode's response signal.

Conflicts of interest

The authors declare no conflict of interest

Acknowledgements

We thank the Swedish Energy Agency (Grant no. 11674-8) for funding this research. We also thank Dr Souvik Roy for providing [Co(dcpgh)(dcpgh₂)]Cl₂ and Ashleigh Castner for the help with the ICP-OES experiments.

References

1. K. E. Dalle, J. Warnan, J. J. Leung, B. Reuillard, I. S. Karmel and E. Reisner, *Chem. Rev.*, 2019, **119**, 2752-2875.
2. Y. Tachibana, L. Vayssieres and J. R. Durrant, *Nature Photonics*, 2012, **6**, 511-518.
3. M. G. Walter, E. L. Warren, J. R. McKone, S. W. Boettcher, Q. Mi, E. A. Santori and N. S. Lewis, *Chem. Rev.*, 2010, **110**, 6446-6473.
4. B. Zhang and L. Sun, *Chem. Soc. Rev.*, 2019, **48**, 2216-2264.
5. M. K. Brennaman, R. J. Dillon, L. Alibabaei, M. K. Gish, C. J. Dares, D. L. Ashford, R. L. House, G. J. Meyer, J. M. Papanikolas and T. J. Meyer, *J. Am. Chem. Soc.*, 2016, **138**, 13085-13102.
6. F. Li, K. Fan, B. Xu, E. Gabrielsson, Q. Daniel, L. Li and L. Sun, *J. Am. Chem. Soc.*, 2015, **137**, 9153-9159.
7. D. L. Ashford, M. K. Gish, A. K. Vannucci, M. K. Brennaman, J. L. Templeton, J. M. Papanikolas and T. J. Meyer, *Chem. Rev.*, 2015, **115**, 13006-13049.
8. Z. Yu, F. Li and L. Sun, *Energy & Environmental Science*, 2015, **8**, 760-775.
9. E. A. Gibson, *Chem. Soc. Rev.*, 2017, **46**, 6194-6209.
10. J. Willkomm, K. L. Orchard, A. Reynal, E. Pastor, J. R. Durrant and E. Reisner, *Chemical Society Reviews*, 2016, **45**, 9-23.
11. E. Benazzi, J. Mallows, G. H. Summers, F. A. Black and E. A. Gibson, *Journal of Materials Chemistry C*, 2019, **7**, 10409-10445.
12. C. J. Wood, G. H. Summers, C. A. Clark, N. Kaeffer, M. Braeutigam, L. R. Carbone, L. D'Amario, K. Fan, Y. Farré, S. Narbey, F. Oswald, L. A. Stevens, C. D. J. Parmenter, M. W. Fay, A. La Torre, C. E. Snape, B. Dietzek, D. Dini, L. Hammarström, Y. Pellegrin, F. Odobel, L. Sun, V. Artero and E. A. Gibson, *PCCP*, 2016, **18**, 10727-10738.
13. L. Tong, A. Iwase, A. Nattestad, U. Bach, M. Weideler, G. Götz, A. Mishra, P. Bäuerle, R. Amal, G. G. Wallace and A. J. Mozer, *Energy & Environmental Science*, 2012, **5**, 9472-9475.
14. P. B. Pati, L. Zhang, B. Philippe, R. Fernández-Terán, S. Ahmadi, L. Tian, H. Rensmo, L. Hammarström and H. Tian, *ChemSusChem*, 2017, **10**, 2480-2495.
15. N. Kaeffer, J. Massin, C. Lebrun, O. Renault, M. Chavarot-Kerlidou and V. Artero, *J. Am. Chem. Soc.*, 2016, **138**, 12308-12311.
16. L. Li, L. Duan, F. Wen, C. Li, M. Wang, A. Hagfeldt and L. Sun, *Chem. Commun.*, 2012, **48**, 988-990.
17. B. Shan, B. D. Sherman, C. M. Klug, A. Nayak, S. L. Marquard, Q. Liu, R. M. Bullock and T. J. Meyer, *The Journal of Physical Chemistry Letters*, 2017, **8**, 4374-4379.
18. B. Shan, A. Nayak, M. K. Brennaman, M. Liu, S. L. Marquard, M. S. Eberhart and T. J. Meyer, *J. Am. Chem. Soc.*, 2018, DOI: 10.1021/jacs.8b03453.
19. K. Fan, F. Li, L. Wang, Q. Daniel, E. Gabrielsson and L. Sun, *PCCP*, 2014, **16**, 25234-25240.
20. M. A. Gross, C. E. Creissen, K. L. Orchard and E. Reisner, *Chemical Science*, 2016, **7**, 5537-5546.
21. Z. Ji, M. He, Z. Huang, U. Ozkan and Y. Wu, *J. Am. Chem. Soc.*, 2013, **135**, 11696-11699.
22. L. J. Antila, P. Ghamgosar, S. Maji, H. Tian, S. Ott and L. Hammarström, *ACS Energy Letters*, 2016, **1**, 1106-1111.
23. S. Lyu, J. Massin, M. Pavone, A. B. Muñoz-García, C. Labrugère, T. Toupance, M. Chavarot-Kerlidou, V. Artero and C. Olivier, *ACS Applied Energy Materials*, 2019, **2**, 4971-4980.
24. B. van den Bosch, J. A. Rombouts, R. V. A. Orru, J. N. H. Reek and R. J. Detz, *ChemCatChem*, 2016, **8**, 1392-1398.
25. B. Shan, A. K. Das, S. Marquard, B. H. Farnum, D. Wang, R. M. Bullock and T. J. Meyer, *Energy & Environmental Science*, 2016, **9**, 3693-3697.
26. K. L. Materna, N. Lalaoui, J. A. Laureanti, A. P. Walsh, B. P. Rimgard, R. Lomoth, A. Thapper, S. Ott, W. J. Shaw, H. Tian and L. Hammarström, *ACS Applied Materials & Interfaces*, 2020, **12**, 4501-4509.
27. L. D'Amario, J. Fohlinger, G. Boschloo and L. Hammarström, *Chemical Science*, 2018, **9**, 223-230.
28. S. Mori, S. Fukuda, S. Sumikura, Y. Takeda, Y. Tamaki, E. Suzuki and T. Abe, *The Journal of Physical Chemistry C*, 2008, **112**, 16134-16139.
29. L. D'Amario, R. Jiang, U. B. Cappel, E. A. Gibson, G. Boschloo, H. Rensmo, L. Sun, L. Hammarström and H. Tian, *ACS Applied Materials & Interfaces*, 2017, **9**, 33470-33477.
30. L. D'Amario, L. J. Antila, B. Pettersson Rimgard, G. Boschloo and L. Hammarström, *The Journal of Physical Chemistry Letters*, 2015, **6**, 779-783.
31. F. Li, R. Xu, C. Nie, X. Wu, P. Zhang, L. Duan and L. Sun, *Chem. Commun.*, 2019, **55**, 12940-12943.
32. C. E. Creissen, J. Warnan and E. Reisner, *Chemical Science*, 2018, **9**, 1439-1447.
33. C. E. Creissen, J. Warnan, D. Antón-García, Y. Farré, F. Odobel and E. Reisner, *ACS Catalysis*, 2019, **9**, 9530-9538.
34. K. A. Click, D. R. Beauchamp, Z. Huang, W. Chen and Y. Wu, *J. Am. Chem. Soc.*, 2016, **138**, 1174-1179.
35. D. A. Hoogeveen, M. Fournier, S. A. Bonke, X.-Y. Fang, A. J. Mozer, A. Mishra, P. Bäuerle, A. N. Simonov and L. Spiccia, *Electrochim. Acta*, 2016, **219**, 773-780.
36. S. Lyu, Y. Farré, L. Ducasse, Y. Pellegrin, T. Toupance, C. Olivier and F. Odobel, *RSC Advances*, 2016, **6**, 19928-19936.

37. R. J. Kamire, M. B. Majewski, W. L. Hoffeditz, B. T. Phelan, O. K. Farha, J. T. Hupp and M. R. Wasielewski, *Chemical Science*, 2017, **8**, 541-549.
38. N. Kaëffer, C. D. Windle, R. Brisse, C. Gablin, D. Leonard, B. Jusselme, M. Chavarot-Kerlidou and V. Artero, *Chemical Science*, 2018, **9**, 6721-6738.
39. H. Li, F. Li, B. Zhang, X. Zhou, F. Yu and L. Sun, *J. Am. Chem. Soc.*, 2015, **137**, 4332-4335.
40. L. Sévery, J. Szczerbiński, M. Taskin, I. Tuncay, F. Brandalise Nunes, C. Cignarella, G. Tocci, O. Blacque, J. Osterwalder, R. Zenobi, M. Iannuzzi and S. D. Tilley, *Nature Chemistry*, 2021, **13**, 523-529.
41. N. Lalaoui, P. Rousselot-Pailley, V. Robert, Y. Mekmouche, R. Villalonga, M. Holzinger, S. Cosnier, T. Tron and A. Le Goff, *ACS Catalysis*, 2016, **6**, 1894-1900.
42. C. Gutiérrez-Sánchez, M. Pita, C. Vaz-Domínguez, S. Shleev and A. L. De Lacey, *Journal of the American Chemical Society*, 2012, **134**, 17212-17220.
43. B. I. Ipe, K. G. Thomas, S. Barazzouk, S. Hotchandani and P. V. Kamat, *The Journal of Physical Chemistry B*, 2002, **106**, 18-21.
44. A. Kotiaho, R. M. Lahtinen, N. V. Tkachenko, A. Efimov, A. Kira, H. Imahori and H. Lemmetyinen, *Langmuir*, 2007, **23**, 13117-13125.
45. R. K. Gupta and A. S. Achalkumar, *The Journal of Organic Chemistry*, 2018, **83**, 6290-6300.
46. M. T. Rojas, R. Koeniger, J. F. Stoddart and A. E. Kaifer, *J. Am. Chem. Soc.*, 1995, **117**, 336-343.
47. J. Liu, W. Ong, E. Román, M. J. Lynn and A. E. Kaifer, *Langmuir*, 2000, **16**, 3000-3002.
48. S. Roy and E. Reisner, *Angew. Chem.*, 2019, **131**, 12308-12312.
49. G. Chen and M. Jiang, *Chem. Soc. Rev.*, 2011, **40**, 2254-2266.
50. R. J. Lindquist, B. T. Phelan, A. Reynal, E. A. Margulies, L. E. Shoer, J. R. Durrant and M. R. Wasielewski, *Journal of Materials Chemistry A*, 2016, **4**, 2880-2893.
51. C. Zhou, J. Huang and Y. Yan, *Soft Matter*, 2016, **12**, 1579-1585.
52. S. Roy, Z. Huang, A. Bhunia, A. Castner, A. K. Gupta, X. Zou and S. Ott, *J. Am. Chem. Soc.*, 2019, **141**, 15942-15950.
53. J. R. Aranzaes, M.-C. Daniel and D. Astruc, *Canadian Journal of Chemistry*, 2006, **84**, 288-299.
54. B. Xu, L. Tian, A. S. Etman, J. Sun and H. Tian, *Nano Energy*, 2019, **55**, 59-64.
55. Y. Farré, F. Maschietto, J. Föhlinger, M. Wykes, A. Planchat, Y. Pellegrin, E. Blart, I. Ciofini, L. Hammarström and F. Odobel, *ChemSusChem*, 2020, **13**, 1844-1855.
56. F. Würthner, C. R. Saha-Möller, B. Fimmel, S. Ogi, P. Leowanawat and D. Schmidt, *Chem. Rev.*, 2016, **116**, 962-1052.
57. F. Odobel, Y. Farré, F. Maschietto, J. Föhlinger, M. Wykes, A. Planchat, Y. Pellegrin, E. Blart, I. Ciofini and L. Hammarström, *ChemSusChem*, **n/a**.
58. M. Brust, M. Walker, D. Bethell, D. J. Schiffrin and R. Whyman, *J. Chem. Soc., Chem. Commun.*, 1994, DOI: 10.1039/C39940000801, 801-802.
59. O. Swiech, R. Bilewicz and E. Megiel, *RSC Advances*, 2013, **3**, 5979-5986.
60. A. McNeillie, D. H. Brown, W. E. Smith, M. Gibson and L. Watson, *J. Chem. Soc., Dalton Trans.*, 1980, DOI: 10.1039/DT9800000767, 767-770.
61. C. Paun, G. Stowik, E. Lewin and J. Sá, *RSC Advances*, 2016, **6**, 87564-87568.
62. N. Queyriaux, R. A. Wahyuono, J. Fize, C. Gablin, M. Wächtler, E. Martinez, D. Léonard, B. Dietzek, V. Artero and M. Chavarot-Kerlidou, *The Journal of Physical Chemistry C*, 2017, **121**, 5891-5904.
63. C. D. Windle, J. Massin, M. Chavarot-Kerlidou and V. Artero, *Dalton Transactions*, 2018, **47**, 10509-10516.
64. K. L. Materna, A. M. Beiler, A. Thapper, S. Ott, H. Tian and L. Hammarström, *ACS Applied Materials & Interfaces*, 2020, **12**, 31372-31381.
65. D. A. Hoogeveen, M. Fournier, S. A. Bonke, A. Nattestad, A. Mishra, P. Bäuerle, L. Spiccia, A. J. Mozer and A. N. Simonov, *The Journal of Physical Chemistry C*, 2017, **121**, 25836-25846.
66. L. Tian, R. Tyburski, C. Wen, R. Sun, M. Abdellah, J. Huang, L. D'Amario, G. Boschloo, L. Hammarström and H. Tian, *J. Am. Chem. Soc.*, 2020, **142**, 18668-18678.
67. Z. Liu, D. Xiong, X. Xu, Q. Arooj, H. Wang, L. Yin, W. Li, H. Wu, Z. Zhao, W. Chen, M. Wang, F. Wang, Y. B. Cheng and H. He, *ACS Appl Mater Interfaces*, 2014, **6**, 3448-3454.
68. M. Abdellah, A. M. El-Zohry, L. J. Antila, C. D. Windle, E. Reisner and L. Hammarstrom, *J Am Chem Soc*, 2017, **139**, 1226-1232.
69. M. Abdellah, S. Zhang, M. Wang and L. Hammarström, *ACS Energy Letters*, 2017, **2**, 2576-2580.
70. A. Nattestad, A. J. Mozer, M. K. R. Fischer, Y. B. Cheng, A. Mishra, P. Bäuerle and U. Bach, *Nature Materials*, 2009, **9**, 31.